Comparing relativistic and nonrelativistic quark pair creation models

Xiu-Li Gao, Yu-Hui Zhou, Bin Wu, and Zhi-Yong Zhou*

School of Physics, Southeast University, Nanjing 211189, People's Republic of China

(Received 24 April 2026; accepted 25 September 2026; published 26 October 2026)

We investigate the strong decay properties of light unflavored and strange mesons within a relativistic quark-pair-creation (QPC) framework and compare the results with those obtained in the conventional nonrelativistic QPC model. Our analysis shows that, within the present theoretical and experimental uncertainties, the relativistic QPC model yields predictions for strong decay widths of comparable overall quality to those of the nonrelativistic QPC model. This indicates that the nonrelativistic QPC approach remains adequate for estimating decay widths in most practical applications. Nevertheless, owing to the inclusion of Lorentz boosts and Wigner rotations, the relativistic QPC model exhibits a stronger suppression of the energy-dependent decay amplitudes in the high-energy region. This feature reflects the off-shell behavior of the QPC vertex, rather than the on-shell partial decay widths. It may become relevant in unquenched quark-model studies, where the energy-dependent QPC vertex enters meson-loop self-energy corrections and mass shifts through integrations over a broad energy region.

DOI: 10.1103/g1gk-mktl

I. INTRODUCTION

Strong hadronic decays provide an important window on the nonperturbative dynamics of quantum chromodynamics (QCD). Since these processes typically occur at energy scales where perturbative methods are not applicable, a number of phenomenological approaches have been developed to describe transitions between hadronic states. Among them, the quark-pair-creation (QPC) model, more commonly known as the $^3P_0$ model, has long been used as a standard framework for Okubo-Zweig-Iizuka (OZI)-allowed strong decays of mesons and baryons [1–8].

In the QPC model, the decay is assumed to proceed through the creation of an additional quark-antiquark pair from the vacuum with quantum numbers $J^{PC} = 0^{++}$. In spectroscopic notation, this corresponds to a spin-triplet P-wave $q\bar{q}$ pair, which gives the model its name. The created pair then recombines with the constituents of the parent hadron to form the final-state hadrons. Although phenomenological in nature, this construction has been found to provide a useful description of a broad class of OZI-allowed transitions.

The model was first proposed by Micu [1] and was subsequently developed in a systematic way by Le Yaouanc and collaborators, who formulated it in terms of explicit spin, flavor, and spatial wave functions. As constituent quark models became more widely used, the QPC framework was adopted extensively in studies of conventional mesons and baryons, owing both to its relative simplicity and to its reasonable phenomenological performance in many applications [5–7,9–22].

At the same time, considerable effort has been devoted to understanding the microscopic origin of the $^3P_0$ vertex. One frequently discussed interpretation relates the pair-creation operator to the Lorentz structure of confinement: if the confining interaction contains a dominant scalar component, then pair creation with vacuum quantum numbers 0^{++} can arise rather naturally. Related analyses have also attempted to connect the phenomenological decay operator with more microscopic interquark interactions, often through suitable nonrelativistic reductions of the underlying dynamics [23,24].

The QPC model has also been widely applied in heavy-quark spectroscopy, where it is commonly used to estimate open-flavor strong decay widths of charmonium, bottomonium, and heavy-light mesons. In such systems, the nonrelativistic approximation is often expected to be more reliable. For light hadrons and highly excited states, however, its applicability is less clear since larger internal momenta, stronger recoil effects, and relativistic spin couplings may become more important.

In its conventional implementation, the QPC model is essentially nonrelativistic: hadron wave functions are usually taken from nonrelativistic or relativized quark potential models, and the decay operator is typically evaluated with nonrelativistic kinematics, regardless of whether the final-state mesons are moving at relativistic velocities. It is therefore worthwhile to examine whether a relativistic treatment may affect phenomenological predictions in these regimes, which is still absent in the literature.

*Contact author: zhouzhy@seu.edu.cn

Published by the American Physical Society under the terms of the Creative Commons Attribution 4.0 International license. Further distribution of this work must maintain attribution to the author(s) and the published article's title, journal citation, and DOI. Funded by SCOAP³.

Beyond the calculation of isolated partial widths, the QPC mechanism has also been used extensively in unquenched quark models, where it couples valence quark-model states to meson-meson continuum channels and thereby generates self-energy corrections, configuration mixing, and continuum components in hadron wave functions [25–27]. In such applications, not only the on-shell decay widths but also the off-shell energy dependence of the vertex functions may become relevant, which makes the role of relativistic effects of particular interest.

In this work, we present an exploratory comparison between the conventional nonrelativistic QPC model and a relativistic formulation developed along the lines of Refs. [28,29]. Using meson wave functions from the Godfrey-Isgur (GI) model, we calculate partial decay widths for a representative set of meson states in both approaches. We find that the two formulations generally give similar results for many channels, while the relativistic treatment appears to provide some improvement for certain highly excited states. We also compare the corresponding vertex functions as functions of the center-of-mass energy and find that the relativistic formulation exhibits a noticeably milder high-energy behavior. This feature may be relevant in applications where the energy dependence of the hadronic vertices plays a significant role.

This paper is organized as follows. In Sec. II, we briefly review the nonrelativistic QPC model in Sec. II A and the relativistic QPC model in Sec. II B. Numerical results for the strong decays of light and strange mesons are presented in Sec. III, where they are compared with available experimental data and with the predictions of the nonrelativistic model. Finally, Sec. IV contains our conclusions. Appendix A presents the construction of the Lorentz-invariant two-particle state, while Appendix B summarizes the masses and widths of the selected meson states.

II. THE QPC MODEL

A. The nonrelativistic version

In the conventional QPC model [1,7,23], a quark-antiquark pair with the quantum number $J^{PC}=0^{++}$ is created from the vacuum, and then they are combined with the quark and antiquark in the initial hadron state to form the final states. For the meson case, the wave function of a mock meson A is defined by

$$\begin{aligned}&\left|A\left(n_A{}^{2S_A+1}L_{AJ_AM_{J_A}}\right)(\mathbf{P}_A)\right\rangle\\&\equiv\sum_{M_{L_A},M_{S_A}}\langle L_AM_{L_A}S_AM_{S_A}|J_AM_{J_A}\rangle\\&\quad\times\int \mathrm{d}^3\mathbf{p}_A\psi^A_{L_AM_{L_A}}(\mathbf{p}_A)\chi^{12}_{S_AM_{S_A}}\phi^{12}_A\omega^{12}_A\\&\quad\times\left|q_1\left(\frac{\mu_1}{\mu_1+\mu_2}\mathbf{P}_A+\mathbf{p}_A\right)\bar{q}_2\left(\frac{\mu_2}{\mu_1+\mu_2}\mathbf{P}_A-\mathbf{p}_A\right)\right\rangle.\end{aligned}\tag{1}$$

In this representation, the c.m. momentum of meson A denotes $\mathbf{P}_A$, and the relative momentum of the quark-antiquark pair $\mathbf{p}_A$ is integrated over all values. $|S_A,M_{S_A}\rangle$, $|L_A,M_{L_A}\rangle$, and $|J_A,M_{J_A}\rangle$ are, respectively, spin, relative angular momentum, and total angular momentum with their third components. $\chi^{12}_{S_AM_{S_A}}$, ϕ^{12}_A and ω^{12}_A are spin, flavor, and color wave functions of the quark pair, respectively. $\psi^A_{L_AM_{L_A}}(\mathbf{p}_A)$ is the spatial wave function of c.m. frame in momentum space; μ_1 and μ_2 are the masses of the quark and antiquark, and $|q_1(\mathbf{p}_1)\bar{q}_2(\mathbf{p}_2)\rangle$ is the plane-wave state of a free quark and antiquark. Normalizations of the mock meson could be chosen as

$$\left\langle A(\mathbf{P}_i)|A(\mathbf{P}_j)\right\rangle=\delta^3\left(\mathbf{P}_i-\mathbf{P}_j\right).\tag{2}$$

Notice that the normalization is chosen for convenience of the later comparison with the relativistic version.

For the meson decay $A\to BC$, with quark labels denoted as $(12)\to(14)+(32)$, the S-matrix reads

$$\begin{aligned}\langle BC|S|A\rangle&=I-2\pi i\delta\left(E_f-E_i\right)\langle BC|T|A\rangle\\&=I-2\pi i\delta\left(E_f-E_i\right)\delta^3(\mathbf{P}_B+\mathbf{P}_C-\mathbf{P}_A)\\&\quad\times\mathcal{M}^{M_{J_A}M_{J_B}M_{J_C}},\end{aligned}\tag{3}$$

with the transition operator T_{NR} expressed as

$$\begin{aligned}T_{\mathrm{NR}}=&-3\gamma_{\mathrm{NR}}\sum_m\langle 1m1-m|00\rangle\int \mathrm{d}^3\mathbf{p}_3\mathrm{d}^3\mathbf{p}_4\delta^3(\mathbf{p}_3+\mathbf{p}_4)\\&\times\mathcal{Y}^m_1\left(\frac{\mathbf{p}_3-\mathbf{p}_4}{2}\right)\chi^{34}_{1-m}\phi^{34}_0\omega^{34}_0b^\dagger_3(\mathbf{p}_3)d^\dagger_4(\mathbf{p}_4),\end{aligned}\tag{4}$$

where γ_{NR} represents the production strength parameter. $b^\dagger_3(\mathbf{p}_3)$ and $d^\dagger_4(\mathbf{p}_4)$ are the creation operators of quark and antiquark. χ^{34}_{1-m}, ϕ^{34}_0, ω^{34}_0 represents spin triplet, flavor singlet, and color singlet wave functions. $\mathcal{Y}^m_l(\mathbf{p})=p^lY^m_l(\theta_p,\phi_p)$ is a solid harmonic that gives the momentum-space distribution of the created pair. All these elements are used to ensure the created quark and antiquark to possess the vacuum quantum numbers.

The helicity amplitude could be obtained by standard derivations as

$$
\begin{aligned}
&\mathcal{M}^{M_{J_A}M_{J_B}M_{J_C}} \\
&= \gamma_{\mathrm{NR}} \sum_{\substack{M_{L_A},M_{S_A},M_{L_B},M_{S_B} \\ M_{L_C},M_{S_C},m}} \langle L_A M_{L_A} S_A M_{S_A} | J_A M_{J_A} \rangle \\
&\quad \times \langle L_B M_{L_B} S_B M_{S_B} | J_B M_{J_B} \rangle \langle L_C M_{L_C} S_C M_{S_C} | J_C M_{J_C} \rangle \\
&\quad \times \langle 1 m 1 - m | 00 \rangle \left\langle \chi^{14}_{S_B M_{S_B}} \chi^{32}_{S_C M_{S_C}} | \chi^{12}_{S_A M_{S_A}} \chi^{34}_{1-m} \right\rangle \\
&\quad \times \left[\left\langle \phi^{14}_B \phi^{32}_C | \phi^{12}_A \phi^{34}_0 \right\rangle I^{M_{L_A} m}_{M_{L_B} L_B}(\mathbf{q}) \right. \\
&\quad \left. + (-1)^{1+S_A+S_B+S_C} \left\langle \phi^{32}_B \phi^{14}_C | \phi^{12}_A \phi^{34}_0 \right\rangle I^{M_{L_A} m}_{M_{L_B} L_B}(-\mathbf{q}) \right], \qquad (5)
\end{aligned}
$$

where $\langle \chi^{14}_{S_B M_{S_B}} \chi^{32}_{S_C M_{S_C}} | \chi^{12}_{S_A M_{S_A}} \chi^{34}_{1-m} \rangle$ is the spin matrix element, and the color matrix element $\langle \omega^{14}_B \omega^{32}_C | \omega^{12}_A \omega^{34}_0 \rangle = 1/3$, canceling the factor 3 in the definition of T operator. The flavor matrix element $\langle \phi^{14}_B \phi^{32}_C | \phi^{12}_A \phi^{34}_0 \rangle = 1/\sqrt{3}$ with the assumption of flavor $SU(3)$ symmetry. The space integral factor is given by

$$
\begin{aligned}
I^{M_{L_A} m}_{M_{L_B} L_B}(\mathbf{q}) = \int \mathrm{d}^3\mathbf{p} \psi^{B*}_{L_B M_{L_B}} \left(\frac{m_3}{m_1 + m_3} \mathbf{q} + \mathbf{p} \right) \\
\times \psi^{C*}_{L_C M_{L_C}} \left(\frac{m_3}{m_2 + m_3} \mathbf{q} + \mathbf{p} \right) \\
\times \psi^{A}_{L_A M_{L_A}}(\mathbf{q} + \mathbf{p}) \mathcal{Y}^m_1(\mathbf{p}), \qquad (6)
\end{aligned}
$$

where we have taken $\mathbf{q} = \mathbf{P}_B = -\mathbf{P}_C$, $\mathbf{p} = \mathbf{p}_3$.

By choosing the momentum $\mathbf{q}$ along the z axis and applying the Jacob-Wick formula [30], the partial wave amplitude is expressed as

$$
\begin{aligned}
M^{SL}(q) = \frac{\sqrt{4\pi(2L+1)}}{2J_A + 1} \\
\times \sum_{M_{J_B}, M_{J_C}} \langle L 0 S (M_{J_B} + M_{J_C}) | J_A (M_{J_B} + M_{J_C}) \rangle \\
\times \langle J_B M_{J_B} J_C M_{J_C} | S (M_{J_B} + M_{J_C}) \rangle \\
\times M^{(M_{J_A} = M_{J_B} + M_{J_C}) M_{J_B} M_{J_C}}(q \hat{z}), \qquad (7)
\end{aligned}
$$

where S denotes total spin, and L denotes the relative angular momentum of final mesons. Thus, the partial decay width of meson A could be calculated through the following formula:

$$
\Gamma^{SL} = 2\pi \frac{q E_B E_C s}{M_A} |M^{SL}|^2, \qquad (8)
$$

where E_B and E_C are energies of B and C in the c.m. frame of A, and $s \equiv 1/(1 + \delta_{BC})$ is the statistical factor when B and C are identical.

B. The relativistic quark pair creation model

In the nonrelativistic QPC model, the relative wave function of the quark-antiquark pair in a meson is defined in the meson rest frame, and Galilean transformations are implicitly assumed in the construction of the decay amplitude. Such a treatment is generally adequate only when the final-state momenta are sufficiently small. For decays involving sizable recoil, however, a proper Lorentz-covariant treatment becomes necessary [28,29]. In the following, we denote a four-momentum by $p = (p^0, \mathbf{p})$, and use $l_c(p)$ to represent the canonical Lorentz boost from the original inertial frame to a frame moving with velocity $\mathbf{v} = -\mathbf{p}/p^0$.

The relativistic mock state of meson A with momentum $\mathbf{p}$ in the lab frame is constructed by applying canonical Lorentz boosts $l_c(p)$ to the quark and antiquark state,

$$
\begin{aligned}
&|A(^{2s_A+1} l_{j_A m_A})(\mathbf{p})\rangle \\
&= \sum_{m_l, m_s, m_1, m_2 m'_1, m'_2} \int d^3\mathbf{k} \psi^A_{l_A m_A}(\mathbf{k}) |\mathbf{p}_1, s_1 m'_1\rangle \\
&\quad \otimes |\mathbf{p}_2, s_2 m'_2\rangle \phi^{12}_A \omega^{12}_A \\
&\quad \times \mathscr{D}^{s_1}_{m'_1 m_1}[r_c(l_c(p), k_1)] \mathscr{D}^{s_2}_{m'_2 m_2}[r_c(l_c(p), k_2)] \\
&\quad \times \langle s_1 s_2 m_1 m_2 | s_A m_{s_A} \rangle \langle l_A s_A m_{l_A} m_{s_A} | j_A m_{j_A} \rangle \\
&\quad \times \left(\frac{\varepsilon_1(\mathbf{p}_1)}{\varepsilon_1(\mathbf{k})} \frac{\varepsilon_2(\mathbf{p}_2)}{\varepsilon_2(-\mathbf{k})} \frac{W_{12}(\mathbf{k})}{E_{12}(\mathbf{p}, \mathbf{k})} \right)^{1/2}, \qquad (9)
\end{aligned}
$$

where p_1 and p_2 denotes the four-momentum of the quark and antiquark in the meson in the lab frame and k_1 and k_2 their four-momentum in the c.m. frame of the meson. $p \equiv (p^0, \mathbf{p}) = p_1 + p_2 = (\varepsilon_1(\mathbf{p}_1 + \varepsilon_2(\mathbf{p}_2), \mathbf{p}_1 + \mathbf{p}_2)$ and

$$
\begin{aligned}
\varepsilon_i(\mathbf{k}) &= (\mathbf{k}^2 + \mu_i^2)^{1/2}, \\
W_{12}(\mathbf{k}) &= \varepsilon_1(\mathbf{k}) + \varepsilon_2(-\mathbf{k}), \\
E_{12}(\mathbf{p}, \mathbf{k}) &= (W_{12}(\mathbf{k})^2 + \mathbf{p}^2)^{1/2}. \qquad (10)
\end{aligned}
$$

$r_c(a, p) \equiv l_c^{-1}(ap) a l_c(p)$ is the Wigner rotation; $\mathscr{D}^{(s)}_{m'm}(R)$ is the matrix representation of the rotation R. $\mathbf{k}$ is the relative momentum of quark in the c.m. frame of the meson. The factors are defined so as to obtain the normalization condition

$$
\langle A(^{2s_A+1} l_{j_A m_A})(\mathbf{p}') | A(^{2s_A+1} l_{j_A m_A})(\mathbf{p}) \rangle = \delta^3(\mathbf{p} - \mathbf{p}'). \qquad (11)
$$

Here ψ^A_{lm} is the relative wave function of the $q\bar{q}$ pair in meson A, and its normalization satisfies $\int d^3k |\psi^A_{lm}(\mathbf{k})|^2 = 1$. The detailed derivation of two-particle state angular momentum representation can be found in Appendix A.

The interaction Hamiltonian is obtained from the quantum field theory,

$$
H_I = \gamma \int \mathrm{d}^3 x \bar{\psi}(x) \psi(x), \quad t = 0, \qquad (12)
$$

where $\psi(x)$ denotes the Dirac field operator defined at the space-time point x, and an instantaneous form is used. The transition operator T_{RL} is derived and written down as [28]

$$\begin{aligned}T_{\mathrm{RL}} = &-\sqrt{8\pi}\gamma_{\mathrm{RL}}\int\frac{d^3\mathbf{p}_3 d^3\mathbf{p}_4}{\sqrt{\varepsilon_3(\mathbf{p}_3)\varepsilon_4(\mathbf{p}_4)}}\delta^{(3)}(\mathbf{p}_3+\mathbf{p}_4)\\ &\times\sum_{m,m_3,m_4}\langle 1m,1-m|00\rangle\mathscr{Y}_1^m\left(\frac{\mathbf{p}_3-\mathbf{p}_4}{2}\right)\\ &\times\left\langle\frac{1}{2}m_3,\frac{1}{2}m_4\middle|1,-m\right\rangle\\ &\times\phi_0^{34}\omega_0^{34}b^\dagger_{m_3}(\mathbf{p}_3)d^\dagger_{m_4}(\mathbf{p}_4),\end{aligned}\tag{13}$$

where the notations are similarly defined as in Eq. (4). Because the interaction Hamiltonian is defined at equal time, the integration variables in Eq. (13) are restricted to the three-momenta of the created quark and antiquark, rather than independent four-momenta. Their zeroth components are dictated by the on-shell condition $p_i^0=\varepsilon_i(\mathbf{p}_i)=\sqrt{\mathbf{p}_i^2+m_i^2}$, precluding independent integration. This formalism systematically incorporates essential relativistic effects, such as relativistic normalization, Lorentz boost kinematics and spin transformations via Wigner rotations. The helicity amplitude in the c.m. frame of meson A is obtained as

$$\begin{aligned}&\mathscr{M}^{m_{j_A}m_{j_B}m_{j_C}}(\mathbf{q})\\ &=\sum_{m_{l_B}m_{s_B}m_{l_C}m_{s_C}m_{l_A}m_{s_A}m}\left\langle l_As_Am_{l_A}m_{s_A}|j_Am_{j_A}\right\rangle\left\langle l_Bs_Bm_{l_B}m_{s_B}|j_Bm_{j_B}\right\rangle\left\langle l_Cs_Cm_{l_C}m_{s_C}|j_Cm_{j_C}\right\rangle\langle 1,m,1,-m|0,0\rangle\\ &\times\Bigg\{\langle\phi_B^{14}\phi_C^{32}|\phi_0^{34}\phi_A^{12}\rangle\int\mathrm{d}^3\mathbf{k}\,\frac{(-\sqrt{8\pi}\gamma_{\mathrm{RL}}/3)}{\varepsilon_3(\mathbf{p}_3)}\psi^{B*}_{l_Bm_{l_B}}(\mathbf{k})\psi^{C*}_{l_Cm_{l_C}}(\mathbf{k}')\psi^{A}_{l_Am_{l_A}}(\mathbf{p}_1)\mathcal{Y}_1^m(\mathbf{p}_3)\\ &\times\sum_{m_1m_4m_3m_2m_1'm_4'm_3'm_2'}\langle s_1s_2m_1'm_2'|s_Am_{s_A}\rangle\langle s_1s_4m_1m_4|s_Bm_{s_B}\rangle\langle s_3s_2m_3m_2|s_Cm_{s_C}\rangle\left\langle s_3s_4m_3'm_4'|1,-m\right\rangle\\ &\times\mathscr{D}^{(1/2)*}_{m_1'm_1}[r_c(l_c(q_1),k_1)]\mathscr{D}^{(1/2)*}_{m_4'm_4}[r_c(l_c(q_1),k_4)]\mathscr{D}^{(1/2)*}_{m_3'm_3}[r_c(l_c(q_2),k_3)]\mathscr{D}^{(1/2)*}_{m_2'm_2}[r_c(l_c(q_2),k_2)]\\ &\times\left(\frac{\varepsilon_1(\mathbf{p}_1)}{\varepsilon_1(\mathbf{k})}\frac{\varepsilon_4(\mathbf{p}_4)}{\varepsilon_4(\mathbf{k})}\frac{W_{14}(\mathbf{k})}{E_{14}(\mathbf{q},\mathbf{k})}\right)^{1/2}\left(\frac{\varepsilon_3(\mathbf{k}')}{\varepsilon_3(\mathbf{p}_3)}\frac{\varepsilon_2(\mathbf{k}')}{\varepsilon_2(\mathbf{p}_2)}\frac{E_{32}(-\mathbf{q},\mathbf{k}')}{W_{32}(\mathbf{k}')}\right)^{1/2}\\ &+\langle\phi_B^{32}\phi_C^{14}|\phi_0^{34}\phi_A^{12}\rangle\int\mathrm{d}^3\mathbf{k}'\,\frac{(-\sqrt{8\pi}\gamma_{\mathrm{RL}}/3)}{\varepsilon_3(\mathbf{p}_3)}\psi^{B*}_{l_Bm_{l_B}}(\mathbf{k}')\psi^{C*}_{l_Cm_{l_C}}(\mathbf{k})\psi^{A}_{l_Am_{l_A}}(\mathbf{p}_1)\mathscr{Y}_1^m(\mathbf{p}_3)\\ &\times\sum_{m_1m_4m_3m_2m_1'm_4'm_3'm_2'}\langle s_1s_2m_1'm_2'|s_Am_{s_A}\rangle\langle s_3s_2m_3m_2|s_Bm_{s_B}\rangle\langle s_1s_4m_1m_4|s_Cm_{s_C}\rangle\langle s_3s_4m_3'm_4'|1,-m\rangle\\ &\times\mathscr{D}^{(1/2)*}_{m_3'm_3}[r_c(l_c(q_1),k_3)]\mathscr{D}^{(1/2)*}_{m_2'm_2}[r_c(l_c(q_1),k_2)]\mathscr{D}^{(1/2)*}_{m_1'm_1}[r_c(l_c(q_2),k_1)]\mathscr{D}^{(1/2)*}_{m_4'm_4}[r_c(l_c(q_2),k_4)]\\ &\times\left(\frac{\varepsilon_3(\mathbf{p}_3)}{\varepsilon_3(\mathbf{k}')}\frac{\varepsilon_2(\mathbf{p}_2)}{\varepsilon_2(\mathbf{k}')}\frac{W_{32}(\mathbf{k}')}{E_{32}(\mathbf{q},\mathbf{k}')}\right)^{1/2}\left(\frac{\varepsilon_1(\mathbf{k})}{\varepsilon_1(\mathbf{p}_1)}\frac{\varepsilon_4(\mathbf{k})}{\varepsilon_4(\mathbf{p}_4)}\frac{E_{14}(-\mathbf{q},\mathbf{k})}{W_{14}(\mathbf{k})}\right)^{1/2}\Bigg\},\end{aligned}\tag{14}$$

where the factor $1/3$ comes from the overlap of the color wave functions. $\mathbf{k}$ is the three-momentum of quark 1 in the c.m. frame of 14 systems, and $\mathbf{k}'$ is the three-momentum of antiquark 3 in the c.m. frame of 32 systems. If quark 1 and antiquark 2 are of the same mass, then $\mathbf{k}=\mathbf{k}'$, and the normalization factors will cancel. $\mathbf{p}_1$ is the three-momentum of the quark 1 in the c.m. frame of meson A, and $\mathbf{q}$ is the three-momentum of meson B in the c.m. frame of A. q_1 and q_2 represent the four-momenta of mesons B and C, respectively. In this formula, there is also only one parameter, γ_{RL}, to represent the production strength from the vacuum.

The transformation from helicity amplitudes to partial-wave amplitudes is carried out using the Jacob-Wick formula, in the same manner as in Eq. (7), after which the decay width is obtained from Eq. (8). It should be noted that, in the relativistic formulation [cf. Eq. (14)], the spatial and spin degrees of freedom are intertwined in the integration over the relative momentum $\mathbf{k}$ or $\mathbf{k}'$. Consequently, unlike in the nonrelativistic case, these contributions cannot, in general, be factorized.

III. NUMERICAL ANALYSES AND DISCUSSIONS

To compare the predictive power of the two versions of the QPC models, one must adopt a specific description of the wave functions for both the initial and final mesons.

In the present work, we employ the GI model [31], which has achieved broad phenomenological success in meson spectroscopy across both light and heavy flavor sectors, particularly for states below the open-flavor thresholds. Since the GI model is widely regarded as a benchmark framework for hadron spectroscopy, utilizing it as a common meson-structure input for both the nonrelativistic (NR)QPC and relativistic (R)QPC calculations allows us to isolate the effects of the different decay approaches, rather than conflating them with variations in the bound-state wave functions. This strategy provides a controlled basis for comparing the nonrelativistic and relativistic QPC formulations on an equal footing. If we were to introduce a completely different set of purely nonrelativistic wave functions exclusively for the NRQPC calculation, then any observed discrepancies in the predicted decay widths could be ambiguously attributed to either the mismatch in the wave functions or the absence of relativistic decay dynamics. This would inherently entangle the bound-state effects with the decay mechanism, thereby obscuring the true physical conclusions.

At the same time, fixing the meson wave functions to those of a well-known spectroscopic model prevents the introduction of arbitrary flexibility. The necessary compromise, however, is that one cannot retune the wave functions to optimize agreement with experimental partial widths for individual channels. Therefore, the quantitative results reported below are intended to illustrate the relative behavior of the nonrelativistic and relativistic QPC formulations within a shared phenomenological framework, rather than to serve as a definitive evaluation of their absolute precision.

The pair-creation strength parameters in the NRQPC and RQPC models, denoted by γ_{NR} and γ_{RL}, respectively, are both free parameters, and there is no *a priori* relation connecting them. Because the spatial wave functions are strictly fixed to those of the GI's model, γ represents the sole adjustable degree of freedom in each formulation. To facilitate a robust and direct comparison, we adopt two kinds of calibration schemes. In the first scheme, we determine the γ_{NR} and γ_{RL} individually by calibrating against the well-measured decay width of the ρ meson and, subsequently, use these values to predict the partial widths of the remaining states. In the second scheme, we determine the optimal γ parameter through a global fit to the experimental decay widths of a selected set of well-established mesons. The fitted sample consists of light-meson states for which experimentally measured two-body partial widths are available in the Particle Data Group (PDG) compilation [32]. The light unflavored scalar resonances, such as the f_0 and a_0 states, are not included in the present analysis. This is mainly because these states typically have large decay widths, which can lead to substantial overlap among neighboring resonances, or because their line shapes may be significantly distorted by nearby open thresholds within a relatively narrow mass region [33]. Throughout these calculations, the physical masses of the initial- and final-state mesons are also taken from the latest compilation of PDG to ensure the correct evaluation of the phase space.

For channels involving strange-quark pair creation, we further assume the commonly used empirical suppression

$$\gamma_{s\bar{s}} = \frac{\gamma_{u\bar{u}}}{\sqrt{3}}, \tag{15}$$

which means the $s\bar{s}$ pair is much harder to be created from the vacuum than the $u\bar{u}$ and $d\bar{d}$ and apply the same prescription in both the nonrelativistic and relativistic calculations. This assumption is introduced only to maintain consistency with standard phenomenological practice; it may itself constitute an additional source of model dependence in the predictions for strange-meson decay channels.

We have calculated the strong decay widths for a broad class of mesons, including light unflavored $n\bar{n}$, $s\bar{s}$, and strange $n\bar{s}$ states. The isoscalar mesons, denoted by f and f' as in the PDG table, are treated as mixtures of the nonstrange and strange flavor components. In the $(u\bar{u}, d\bar{d}, s\bar{s})$ basis, the physical states are written as

$$f' = \frac{1}{\sqrt{2}}(u\bar{u} + d\bar{d})\cos\alpha - s\bar{s}\sin\alpha, \tag{16}$$

$$f = \frac{1}{\sqrt{2}}(u\bar{u} + d\bar{d})\sin\alpha + s\bar{s}\cos\alpha, \tag{17}$$

where α is the mixing angle. In the present work, we adopt the ideal-mixing approximation, under which $f' \approx s\bar{s}$ and $f \approx (u\bar{u} + d\bar{d})/\sqrt{2}$ [31].

The $\rho(770)$ meson decays almost entirely into the $\pi\pi$ channel, and its width is measured accurately. Consequently, using this state ensures that no uncertainties from coupled channels are introduced into the calibration. By determining the strength parameters solely from the ρ meson, $M_\rho = 775.26$ MeV and $\Gamma_\rho = 147.4$ MeV, we obtain

$$\gamma_{\mathrm{NR}} = 18.3, \qquad \gamma_{\mathrm{RL}} = 7.2, \tag{18}$$

where the subscripts NR and RL represent the corresponding values in the nonrelativistic version and the relativistic one. Since the ρ decay width has been experimentally measured with high precision, the statistical uncertainty of the γ parameter extracted from it is negligible and therefore omitted. This notation is maintained throughout the remainder of the paper.

TABLE I. The strong decay widths of isovector mesons $(u\bar{d}, 1/\sqrt{2}(u\bar{u}-d\bar{d}), d\bar{u})$ are compared with those of candidates in the PDG. The unit is MeV.

$J^{PC}(n^{2s+1}L_J)$	Decay	$\Gamma_{\rm exp}$ [32]	$\Gamma_{\rm NR}(\gamma_{\rm NR}=18.3/(14.7\pm1.1))$	$\Gamma_{\rm RL}(\gamma_{\rm RL}=7.2/(5.0\pm0.4))$
$1^{--}(1^3S_1)$	$\rho(770)\to\pi\pi$	147.4 ± 0.8	$147/(95\pm14)$	$147/(70\pm11)$
$1^{--}(2^3S_1)$	$\rho(1450)\to\omega\pi$	84.0 ± 12.6	$106/(68\pm10)$	$179/(85\pm14)$
$1^{+-}(1^1P_1)$	$b_1(1235)\to\omega\pi$	142.0 ± 9.0	$134/(86\pm13)$	$147/(70\pm11)$
$1^{++}(1^3P_1)$	$a_1(1260)\to\rho\pi$	234 ± 49	$457/(293\pm44)$	$500/(238\pm38)$
$2^{++}(1^3P_2)$	$a_2(1320)\to\rho\pi$	75.0 ± 4.5	$34/(22\pm3)$	$45/(22\pm4)$
$2^{++}(1^3P_2)$	$a_2(1320)\to\pi\eta$	15.5 ± 1.5	$11/(7\pm1.1)$	$10/(5\pm0.8)$
$2^{++}(1^3P_2)$	$a_2(1320)\to K\bar{K}$	5.2 ± 0.9	$4/(2\pm0.3)$	$4/(2\pm0.3)$
$2^{++}(1^3P_2)$	$a_2(1700)\to K\bar{K}$	4.9 ± 3.2	$0.9/(0.6\pm0.1)$	$0.5/(0.2\pm0.03)$
$2^{-+}(1^1D_2)$	$\pi_2(1670)\to f_2(1270)\pi$	145.3 ± 9.5	$131/(84\pm13)$	$137/(66\pm11)$
$2^{-+}(1^1D_2)$	$\pi_2(1670)\to\rho\pi$	80.0 ± 10.7	$126/(81\pm12)$	$144/(69\pm11)$
$2^{-+}(1^1D_2)$	$\pi_2(1670)\to K^*(892)\bar{K}$	10.8 ± 3.6	$25/(16\pm2)$	$43/(21\pm3)$
$3^{--}(1^3D_3)$	$\rho_3(1690)\to\pi\pi$	38.0 ± 3.2	$107/(69\pm10)$	$66/(32\pm5)$
$3^{--}(1^3D_3)$	$\rho_3(1690)\to\omega\pi$	25.8 ± 9.8	$20/(13\pm2)$	$24/(11\pm2)$
$3^{--}(1^3D_3)$	$\rho_3(1690)\to K\bar{K}$	2.5 ± 0.4	$2/(1\pm0.1)$	$5/(2\pm0.3)$

For the second calibration scheme, the optimal γ parameters are extracted by minimizing the function $\chi^2=\sum_n(\frac{\Gamma_n^{QPC}-\Gamma_n^{\rm exp}}{\sigma_n})^2$ over the selected set of meson decays. Rather than using the purely experimental uncertainties, which are often statistically very small and would cause certain channels to disproportionately dominate the fit, we assign a uniform tolerance of $\sigma_n=10$ MeV to all channels. This uniform weighting effectively accounts for the inherent theoretical uncertainties typical of phenomenological quark models and ensures a balanced global fit. The resulting best-fit parameters are

$$\gamma_{\rm NR}=14.7\pm1.1,\qquad \gamma_{\rm RL}=5.0\pm0.4. \tag{19}$$

The strong decay widths of the selected light mesons, calculated with the universal γ parameters determined above, are summarized in Tables I–IV. For each entry, the results obtained with the two different γ values are listed together and separated by a "/" symbol. A global inspection of these results indicates that, for most decay channels, the widths predicted by the nonrelativistic and relativistic formulations are numerically similar. However, it must be noted that when the meson wave functions are strictly fixed to the GI model and a single universal γ is employed, the predicted widths generally agree with experimental measurements only at the order-of-magnitude level. This behavior corroborates the findings of Ref. [34], which demonstrated that state-dependent γ values are required to accurately reproduce the strong decay widths across the ρ and ω families.

Furthermore, the extracted value of $\gamma_{\rm NR}=18.3$ from the single $\rho-\pi\pi$ channel calibration is notably larger than the typical values adopted in many nonrelativistic QPC studies. Nevertheless, this large value is entirely consistent with the recognized systematic tendencies of the QPC model. Historically, QPC calculations tend to significantly underestimate the $\rho-\pi\pi$ decay width unless a heavily inflated

TABLE II. The strong decay widths of isoscalar f' mesons are compared with those of candidates in the PDG. The unit is MeV.

$J^{PC}(n^{2s+1}L_J)$	Decay	$\Gamma_{\rm exp}$ [32]	$\Gamma_{\rm NR}(\gamma_{\rm NR}=18.3/(14.7\pm1.1))$	$\Gamma_{\rm RL}(\gamma_{\rm RL}=7.2/(5.0\pm0.4))$
$1^{--}(1^3S_1)$	$\phi(1020)\to K^+K^-$	2.12 ± 0.02	$2/(1\pm0.1)$	$3/(2\pm0.3)$
$2^{++}(1^3P_2)$	$f_2'(1525)\to K\bar{K}$	63.4 ± 6.3	$130/(84\pm13)$	$126/(60\pm10)$
$2^{++}(1^3P_2)$	$f_2'(1525)\to\eta\eta$	7.5 ± 1.8	$24/(15\pm2)$	$20/(10\pm2)$
$3^{--}(1^3D_3)$	$\phi_3(1850)\to K\bar{K}$	31^{+10}_{-8}	$111/(72\pm11)$	$100/(48\pm8)$
$3^{--}(1^3D_3)$	$\phi_3(1850)\to K^*(892)\bar{K}$	56^{+18}_{-14}	$130/(84\pm13)$	$184/(88\pm14)$

TABLE III. The strong decay widths of isoscalar f mesons are compared with those of candidates in the PDG. The unit is MeV.

$J^{PC}(n^{2s+1}L_J)$	Decay	$\Gamma_{\rm exp}$ [32]	$\Gamma_{\rm NR}(\gamma_{\rm NR}=18.3/(14.7\pm1.1))$	$\Gamma_{\rm RL}(\gamma_{\rm RL}=7.2/(5.0\pm0.4))$
$1^{--}(2^3S_1)$	$\omega(1420)\to\rho\pi$	202.7 ± 133.1	$276/(178\pm27)$	$500/(239\pm38)$
$2^{++}(1^3P_2)$	$f_2(1270)\to\pi\pi$	155.8 ± 5.5	$231/(149\pm22)$	$155/(74\pm12)$
$2^{++}(1^3P_2)$	$f_2(1270)\to K\bar{K}$	8.5 ± 0.8	$2/(1\pm0.1)$	$3/(2\pm0.3)$
$4^{++}(1^3F_4)$	$f_4(2050)\to\omega\omega$	40.3 ± 4.7	$165/(106\pm16)$	$349/(167\pm27)$
$4^{++}(1^3F_4)$	$f_4(2050)\to\pi\pi$	35.4 ± 3.8	$92/(59\pm9)$	$59/(28\pm4)$
$4^{++}(1^3F_4)$	$f_4(2050)\to K\bar{K}$	1.6 ± 0.7	$1/(0.6\pm0.1)$	$3/(1.6\pm0.3)$

pair-creation strength is imposed. For instance, in Ref. [18], a nonrelativistic QPC calculation using $\gamma=11.6$ yields $\Gamma_\rho=68.9$ MeV, still falling well short of the experimental width. Similarly, Ref. [23] obtained $\Gamma_\rho\approx79$ MeV using simple harmonic oscillator wave functions ($\beta=0.397$ GeV) and a strength parameter equivalent to $\gamma=0.506\times\sqrt{96\pi}=8.8$. Consequently, forcing the model to fully reproduce the experimental ρ decay width inevitably necessitates a highly elevated $\gamma_{\rm NR}$ parameter.

Ultimately, these results imply that the underlying dynamics of light-meson decays are too complex to be fully captured by a single universal pair-creation parameter. This conclusion is strongly supported by recent nonrelativistic QPC analyses; for example, Ref. [34] showed that simultaneously reproducing the decay widths of the ρ, ρ_3, ω, and ω_3 families requires γ to vary substantially, ranging from roughly 4.14 to 14.6 depending on the specific initial state. Therefore, the order-of-magnitude deviations observed in our results reflect the intrinsic limitations of the universal γ assumption in the light sector.

Based on the present analysis of light-meson decays, several key properties of the QPC formulations can be summarized as follows:

(1) First, it is evident that a single universal pair-creation parameter is insufficient to accurately describe the partial decay widths of all light-meson states simultaneously. Crucially, our results demonstrate that this fundamental limitation cannot be remedied simply by incorporating relativistic effects. As shown in Tables I–IV, when γ is calibrated to precisely fit the ρ meson, the predictions for the $b_1(1235)$, $\pi_2(1670)$, $\omega(1420)$, and $K^*(892)$ are consistent with experimental data. However, sizable discrepancies emerge for other states, generally restricting the agreement to an order of magnitude.

(2) Second, despite deviations in the absolute decay widths, the branching fractions between different

TABLE IV. The strong decay widths of strange mesons $(u\bar{s}, d\bar{s}, s\bar{u}, s\bar{d})$ are compared with those of candidates in the PDG. The unit is MeV.

$J^{PC}(n^{2s+1}L_J)$	Decay	$\Gamma_{\rm exp}$ [32]	$\Gamma_{\rm NR}(\gamma_{\rm NR}=18.3/(14.7\pm1.1))$	$\Gamma_{\rm RL}(\gamma_{\rm RL}=7.2/(5.0\pm0.4))$
$1^{--}(1^3S_1)$	$K^*(892)\to K\pi$	51.4 ± 0.8	$50/(32\pm5)$	$59/(28\pm4)$
$0^{++}(1^3P_0)$	$K_0^*(1430)\to K\pi$	251 ± 80	$1076/(393\pm59)$	$714/(342\pm55)$
$2^{++}(1^3P_2)$	$K_2^*(1430)\to K\pi$	54.4 ± 3.0	$124/(80\pm12)$	$97/(46\pm7)$
$2^{++}(1^3P_2)$	$K_2^*(1430)\to K^*(892)\pi$	26.9 ± 2.1	$51/(33\pm5)$	$66/(32\pm5)$
$2^{++}(1^3P_2)$	$K_2^*(1430)\to K\rho$	9.5 ± 1.0	$17/(11\pm2)$	$28/(14\pm2)$
$2^{++}(1^3P_2)$	$K_2^*(1430)\to K\omega$	3.2 ± 0.9	$5/(3\pm0.4)$	$8/(4\pm0.6)$
$1^{--}(1^3D_1)$	$K^*(1680)\to K\pi$	123.8 ± 43.4	$239/(154\pm23)$	$140/(67\pm11)$
$1^{--}(1^3D_1)$	$K^*(1680)\to K\rho$	100.5 ± 36.8	$125/(80\pm12)$	$132/(63\pm10)$
$1^{--}(1^3D_1)$	$K^*(1680)\to K^*(892)\pi$	95.7 ± 35.0	$127/(82\pm12)$	$111/(53\pm8)$
$3^{--}(1^3D_3)$	$K_3^*(1780)\to K\pi$	30.3 ± 3.6	$84/(54\pm8)$	$63/(30\pm5)$
$3^{--}(1^3D_3)$	$K_3^*(1780)\to K\rho$	49.9 ± 15.4	$50/(32\pm5)$	$74/(35\pm6)$
$3^{--}(1^3D_3)$	$K_3^*(1780)\to K^*(892)\pi$	32.2 ± 8.9	$66/(43\pm6)$	$78/(37\pm6)$
$4^{++}(1^3F_4)$	$K_4^*(2045)\to K\pi$	19.7 ± 3.3	$45/(29\pm4)$	$38/(18\pm3)$
$5^{--}(1^3F_5)$	$K_5^*(2380)\to K\pi$	11.0 ± 3.8	$32/(21\pm3)$	$25/(12\pm2)$

partial widths of the same state are reasonably well described by both QPC models. For instance, although the predicted absolute partial widths of the $a_2(1320)$ to the $\rho\pi$, $\pi\eta$, and $K\bar{K}$ channels are smaller than experimental measurements, both the nonrelativistic and relativistic models successfully capture the experimental branching ratio $\mathcal{B}(a_2(1320) \to \rho\pi):\mathcal{B}(a_2(1320) \to \pi\eta):\mathcal{B}(a_2(1320) \to K\bar{K}) \approx 15:3:1$. Similarly, the ratio $\mathcal{B}(f_2'(1525) \to K\bar{K})/\mathcal{B}(f_2'(1525) \to \eta\eta) \approx 8.4 \pm 2.2$ is well reproduced, with the nonrelativistic and relativistic formulations yielding values of approximately 5.6 and 6.0, respectively.

(3) Finally, for the strange-meson sector, the relativistic and nonrelativistic QPC models also give predictions of comparable overall quality, as shown in Table IV. It should be emphasized that the relativistic formulation does not provide a systematic improvement for every individual decay channel. For example, in the low-lying $K^*(892) \to K\pi$ channel, the relativistic prediction obtained with the global-fit value $\gamma_{\mathrm{RL}} = 5.0$ is 28 MeV, which is significantly smaller than the experimental value of 51.4 MeV. This channel is therefore better described by the nonrelativistic calculation. On the other hand, for several higher-mass strange mesons, such as $K_2^*(1430)$, $K^*(1680)$, $K_3^*(1780)$, $K_4^*(2045)$, and $K_5^*(2380)$, the relativistic QPC model gives a competitive description and, in some channels, improves the agreement with the experimental data, especially when the global-fit value of γ is used. For instance, if the $K^*(892) \to K\pi$ channel is omitted from the diagnostic comparison fit performed exclusively on the strange meson decay channels, then the χ^2/d.o.f drops substantially from approximately 68 to 3. This result indicates that the relativistic formalism might offer a better description of certain higher-mass strange mesons. Nevertheless, this is currently speculative, and comprehensive calculations across a broader range of states are necessary to confirm it.

To further examine whether the general trend depends on the choice of wave functions obtained in a different method, we perform a supplementary calculation using simple harmonic oscillator (SHO) wave functions for several representative decay channels. In momentum space, the SHO wave function is written as

$$\psi^{\mathrm{SHO}}_{nLM_L}(\mathbf{p}) = R^{\mathrm{SHO}}_{nL}(p) Y_{LM_L}(\Omega_p), \tag{20}$$

where the radial wave function is given by

$$R^{\mathrm{SHO}}_{nL}(p) = \frac{(-1)^n(-i)^L}{\beta^{3/2}} \left[\frac{2n!}{\Gamma(n+L+3/2)}\right]^{1/2} \left(\frac{p}{\beta}\right)^L \times \exp\left(-\frac{p^2}{2\beta^2}\right) L_n^{L+1/2}\left(\frac{p^2}{\beta^2}\right), \tag{21}$$

where β is the oscillator parameter in momentum space, and $L_n^{L+1/2}$ denotes the associated Laguerre polynomial. For the SHO wave functions, we adopt the widely used effective parameter $\beta_{\mathrm{eff}} = 0.4$ GeV for light mesons [35]. Indeed, if one evaluates the effective β parameter by matching the rms radii of the states under consideration, the resulting values are also approximately $\beta \approx 0.4$ GeV. Since the SHO and GI wave functions have different spatial structures, the pair-creation strength parameter γ is redetermined separately for the SHO case using the same two calibration schemes as in the GI-wave-function calculation. The resulting parameters are $\gamma_{\mathrm{NR}} = 11.9/9.1$ and $\gamma_{\mathrm{RL}} = 4.2/3.6$ for the SHO wave functions, where the two values correspond to the $\rho \to \pi\pi$ calibration and the global-fit calibration, respectively.

As shown in Table V, after the parameter γ is refitted for the SHO wave functions, the absolute decay widths and their relative patterns are broadly consistent with those obtained using the GI wave functions for the representative channels considered here. In particular, the hierarchy among the selected decay widths and the qualitative comparison between the nonrelativistic and relativistic formulations are not substantially changed. This may indicate that the main conclusions drawn above are not strongly affected by replacing the GI wave functions with a simple SHO parametrization. The remaining deviations should be regarded as part of the intrinsic wave-function dependence of phenomenological QPC calculations.

Taken together, these observations suggest that, while the nonrelativistic QPC model appears to provide an adequate qualitative description for low-lying states and

TABLE V. Comparison of decay widths obtained with GI and SHO wave functions for several representative decay channels. The entries are given as $\Gamma(\gamma_\rho)/\Gamma(\gamma_{\mathrm{fit}})$. For the GI wave functions, $\gamma_{\mathrm{NR}} = 18.3/14.7$ and $\gamma_{\mathrm{RL}} = 7.2/5.0$, while for the SHO wave functions, $\gamma_{\mathrm{NR}} = 11.9/9.1$ and $\gamma_{\mathrm{RL}} = 4.2/3.6$. All decay widths are given in MeV.

Decay channel	Width	NRQPC(GI)	RQPC(GI)	NRQPC(SHO)	RQPC(SHO)
$\rho \to \pi\pi$	147.4 ± 0.8	147/95	147/70	147/86	147/109
$a_2(1320) \to \pi\eta$	15.5 ± 1.5	11/7	10/5	14/8	10/7
$f_2'(1525) \to K\bar{K}$	63.4 ± 6.3	130/84	126/60	160/93	141/105

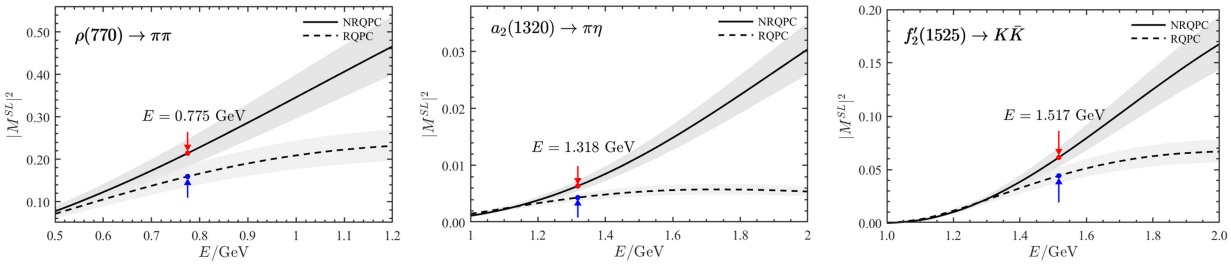


FIG. 1. The squared amplitudes $|M^{SL}|^2$ at the energy of initial mesons for $\rho \to \pi\pi$, $a_2(1320) \to \pi\eta$ and $f_2'(1525) \to K\bar{K}$. Solid curves are obtained from the nonrelativistic QPC model with $\gamma_{\rm NR} = 14.7$, while dashed curves represent the relativistic QPC results with $\gamma_{\rm RL} = 5.0$. The gray bands represent the theoretical uncertainties.

low partial waves, relativistic effects may become increasingly important for highly excited mesons and for decay modes involving large momenta and high orbital angular momentum.

Although the integrated decay widths obtained in the nonrelativistic and relativistic frameworks are numerically similar for most selected channels, the corresponding partial-wave scattering amplitudes $M^{SL}(E)$ can display rather different energy dependence. Such kinds of energy dependence are not paid attention to in the isolated calculation of decay width, because the three-momentum of the final-state mesons is fixed by the parent hadron mass m_A, which is usually set as

$$q = \sqrt{(E^2 - (m_B + m_C)^2)(E^2 - (m_B - m_C)^2)}/2E\Big|_{E=m_A}. \tag{22}$$

When the QPC model is used in unquenched potential models to describe the off-mass-shell coupling vertex functions between a bare state and the relevant scattering channels (see, e.g., Refs. [25,36] and the subsequent literature), the energy-dependence behavior could influence the results. In such applications, the self-energy function is often treated through a dispersion relation, for example, in a relativistic form,

$$\mathrm{Re}\,\Pi(s) = -\frac{1}{\pi}\int_{s_{th}}^{\infty} \frac{\mathrm{Im}\,\Pi(s')}{s - s'}\,ds', \tag{23}$$

where the Mandelstam variable is $s = E^2$, and s_{th} denotes the threshold value. When $\mathrm{Im}\,\Pi(s')$ is modeled within the QPC framework, which is usually written down as $\mathrm{Im}\,\Pi(s) = \rho(s)|M^{SL}(s)|^2$ with $\rho(s)$ representing the kinematic factor proportional to $q(s)/\sqrt{s}$, $\mathrm{Re}\Pi(s)$ may be regarded, at least at the phenomenological level, as contributing to the mass shift of the physical state relative to the bare mass.

As illustrative examples, the quantities $|M^{SL}(E)|^2$ for $\rho \to \pi\pi$, $a_2(1320) \to \pi\eta$ and $f_2'(1525) \to K\bar{K}$ are shown in Fig. 1. When the variable E is fixed at the mass of the parent meson, $|M^{SL}|^2$ is relevant for the partial decay width. One could find from Fig. 1 that the related values in the two formulations are relatively close, which means both frameworks lead to similar predictions for the decay width. As the center-of-mass energy increases, however, the differences between the corresponding squared amplitudes become progressively more pronounced. In the nonrelativistic version, the amplitude rises to a comparatively large maximum before eventually decreasing and approaching zero at energies of order 10 GeV. By contrast, in the relativistic version the variation is considerably more moderate, as indicated by the dashed curve in Fig. 2. This behavior suggests that, even when the integrated widths are similar near the physical mass, the relativistic formulation exhibits a substantially milder high-energy dependence than its nonrelativistic counterpart.

Since the dispersion integral of Eq. (23) extends from threshold to infinity, the resulting mass-shift $\mathrm{Re}\Pi(s)$ can, in principle, be sensitive to the behavior of the transition amplitude over a broad energy range, including regions far above the physical decay point. In conventional nonrelativistic QPC-based analyses, such effects have often been associated with rather sizable mass shifts, sometimes of the order of several hundred MeV. As indicated in Fig. 2, however, the amplitude of relativistic framework displays a comparatively milder energy dependence at high energies. If such a trend remains relevant in self-energy applications, the relativistic formulation may reduce the relative importance of the high-energy region in the dispersion integral.

From this perspective, the slower falloff of $|M^{SL}|^2$ in the nonrelativistic QPC model could enhance high-momentum contributions and thereby increase the sensitivity of the inferred mass shifts to the ultraviolet behavior of the model. By contrast, the relativistic formulation may suppress high-energy strength more efficiently. It means that including Lorentz-boost effects reduces the contribution from the high energy region. Such a relativistic treatment could improve the convergence properties of the self-energy integral and lead to a more stable phenomenological determination of the physical mass. At the same time, it should be kept in mind that such conclusions are necessarily model dependent and may also be influenced by the

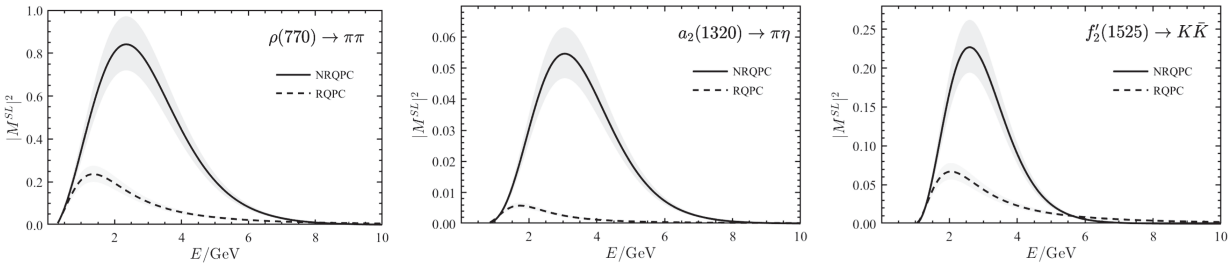


FIG. 2. Comparison of the squared amplitudes $|M^{SL}|^2$ of nonrelativistic and relativistic ones in a larger off-shell energy range for three channels with the same parameters used in Fig. 1. The gray bands represent the theoretical uncertainties.

treatment of subtraction constants, form factors, and wave-function parameters.

IV. SUMMARY

Currently, the nonrelativistic QPC model is extensively used to evaluate hadron decay widths and to calculate transition potentials in coupled-channel models. However, relativistic effects are rarely incorporated in these studies, regardless of whether the final-state mesons are moving at relativistic velocities. The primary objective of this manuscript is to systematically compare the predictive power and theoretical behavior of the nonrelativistic and relativistic QPC formulations—a comparison that has been largely absent in the literature.

In this work, we present a comparative study of the strong decays of light and strange mesons in both the nonrelativistic and relativistic QPC frameworks. The relativistic formulation incorporates meson wave functions from the GI's model, exact kinematical phase space, and Wigner rotations of quark spins, thus providing a more consistent treatment of decays involving sizable internal momenta. Partial-wave decay widths are evaluated for $n\bar{n}$, $n\bar{s}$, and $s\bar{s}$ mesons, including both low-lying and radially excited states such as the K, K^*, and isoscalar f and f' families.

Our analysis yields two main conclusions: First, we find that, for many of the light-meson decay channels considered in this work, the total widths predicted by the relativistic and nonrelativistic QPC models are numerically similar. This implies that the nonrelativistic QPC model can produce practically reasonable decay widths even for relativistically moving final states. We attribute this to the universal pair-creation parameter γ, when fitted to a broad range of states, the relatively large uncertainty and flexibility of γ effectively absorb the omitted relativistic kinematic effects. It also implied that the nonrelativistic version of the QPC model could provide a rapid and practical estimation of the decay width, bypassing the need for more complicated relativistic treatment.

Second, the relativistic formulation generally exhibits a stronger suppression at larger available energies, which should be understood as an off-shell feature of the QPC vertex rather than as a universal improvement of all partial decay widths. This property may become particularly relevant in applications sensitive to the energy dependence of the QPC transition amplitudes, such as coupled-channel analyses and unquenched quark models.

ACKNOWLEDGMENTS

Helpful discussions with Cheng-Qun Pang were appreciated. This work is supported by China National Natural Science Foundation under Contract No. 12375132, No. 11975075.

DATA AVAILABILITY

The data that support the findings of this article are not publicly available. The data are available from the authors upon reasonable request.

APPENDIX A: LORENTZ-INVARIANT TWO-PARTICLE STATE

We adopt the canonical Lorentz boost as the basic building block. We denote a four-momentum by $p = (p^0, \mathbf{p})$ and use $l_c(p)$ to represent the canonical Lorentz boost from the original inertial frame to a frame moving with velocity $\mathbf{v} = -\mathbf{p}/p^0$. If $q = (q^0, \mathbf{q})$ is a four-vector in some original inertial frame, then its image under the canonical boost to the moving frame is written compactly as

$$l_c(p)q = l_c(p)\begin{pmatrix} q^0 \\ \mathbf{q} \end{pmatrix} = \begin{pmatrix} \frac{p^0 q^0 + \mathbf{p}\cdot\mathbf{q}}{W} \\ \mathbf{q} + \frac{\mathbf{p}}{W}\left(\frac{\mathbf{p}\cdot\mathbf{q}}{p^0+W} + q^0\right) \end{pmatrix}, \quad \text{(A1)}$$

where $W = \sqrt{p \cdot p}$. The one-particle momentum-spin state with mass μ, spin s, and third-component m is defined by acting with the unitary representation of this boost on the rest-frame spin eigenstate and including the usual relativistic normalization factor:

$$|\mathbf{p}, sm\rangle = U(l_c(\mathbf{p}))|0, sm\rangle\sqrt{\frac{\mu}{\varepsilon(\mathbf{p})}}, \quad \text{(A2)}$$

with $\varepsilon(\mathbf{p}) = \sqrt{\mathbf{p}^2 + \mu^2}$, $\sqrt{\frac{\mu}{\varepsilon(\mathbf{p})}}$ is the normalization coefficient. Under a general Lorentz transformation a the

one-particle basis transforms with an accompanying Wigner rotation $r_c(a,p)$; the representation matrix element reads [37]

$$U(a)|\mathbf{p},sm\rangle=\sum_{m'}|a\mathbf{p},sm'\rangle\mathscr{D}^{(s)}_{m'm}(r_c(a,p))\sqrt{\frac{\varepsilon(a\mathbf{p})}{\varepsilon(\mathbf{p})}}, \quad \text{(A3)}$$

where $r_c(a,p)=l_c^{-1}(ap)al_c(p)$ is the Wigner rotation, and $\mathscr{D}^{(s)}_{m'm}(r_c(a,p))$ is the standard matrix representation of the rotation $r_c(a,p)$.

Based on the definition of the single-particle state, we construct two-particle (denoted as particle "1" and "2") kinematics by first specifying the c.m. variables [28]. In the c.m. frame the two on-shell four-momenta are

$$k_1=(\varepsilon_1(\mathbf{k}),\mathbf{k}),\qquad k_2=(\varepsilon_2(-\mathbf{k}),-\mathbf{k}),$$
$$\varepsilon_i(\mathbf{k})=\sqrt{\mathbf{k}^2+\mu_i^2},$$

where $\mathbf{k}$ is the three-momentum of particle 1 in the c.m. frame of the two-particle system. Boosting this two-particle configuration to a general total four-momentum $p=(p^0,\mathbf{p})$ by the canonical boost $l_c(p)$ gives the lab-frame single-particle four-momenta $p_i=l_c(p)k_i$ with $p_1+p_2=p$. One may then define a boosted two-particle canonical state by

$$|\mathbf{pk},s_1m_1s_2m_2\rangle=U(l_c(p))|\mathbf{k},s_1m_1\rangle\otimes|-\mathbf{k},s_2m_2\rangle\times\sqrt{\frac{W(\mathbf{k})}{E(\mathbf{p},\mathbf{k})}},$$
$$W(\mathbf{k})=\varepsilon_1(\mathbf{k})+\varepsilon_2(-\mathbf{k}),$$
$$E(\mathbf{p},\mathbf{k})=\sqrt{\mathbf{p}^2+W(\mathbf{k})^2}, \quad \text{(A4)}$$

and the two-particle state mentioned above could be expressed as the combination of the direct product of two single-particle states multiplied with extra factors of the matrix representations for the Wigner rotations of the two particles

$$|\mathbf{pk},s_1s_2m_1m_2\rangle=\sum_{m_1'm_2'}|\mathbf{p}_1,s_1m_1'\rangle\otimes|\mathbf{p}_2,s_2m_2'\rangle\times\mathscr{D}^{s_1}_{m_1'm_1}[r_c(l_c(p),k_1)]\times\mathscr{D}^{s_2}_{m_2'm_2}[r_c(l_c(p),k_2)]\times\left(\frac{\varepsilon_1(\mathbf{p}_1)\varepsilon_2(\mathbf{p}_2)W(\mathbf{k})}{\varepsilon_1(\mathbf{k})\varepsilon_2(-\mathbf{k})E(\mathbf{p},\mathbf{k})}\right)^{1/2}. \quad \text{(A5)}$$

Similarly, one can perform the partial wave decomposition and couple the orbital angular momentum l and total spin s to form the total angular momentum j in the c.m. frame. Then, by boosting to a general frame, one can express the two-particle state in the angular momentum representation as

$$\begin{aligned}|\mathbf{p}klsjm\rangle&=\sum_{m_l,m_s,m_1,m_2}\int d\Omega_{\mathbf{k}}Y_l^{m_l}(\hat{\mathbf{k}})|\mathbf{pk},s_1s_2m_1m_2\rangle\langle s_1s_2m_1m_2|sm_s\rangle\langle lsm_lm_s|jm\rangle\\&=\sum_{m_l,m_s,m_1,m_2,m_1',m_2'}\int d\Omega_{\mathbf{k}}|\mathbf{p}_1,s_1m_1'\rangle\otimes|\mathbf{p}_2,s_2m_2'\rangle Y_l^{m_l}(\hat{\mathbf{k}})\langle s_1s_2m_1m_2|sm_s\rangle\langle lsm_lm_s|jm\rangle\\&\quad\times\mathscr{D}^{s_1}_{m_1'm_1}[r_c(l_c(p),k_1)]\mathscr{D}^{s_2}_{m_2'm_2}[r_c(l_c(p),k_2)]\left(\frac{\varepsilon_1(\mathbf{p}_1)\varepsilon_2(\mathbf{p}_2)W(\mathbf{k})}{\varepsilon_1(\mathbf{k})\varepsilon_2(-\mathbf{k})E(\mathbf{p},\mathbf{k})}\right)^{1/2}, \quad \text{(A6)}\end{aligned}$$

where k is the magnitude of the three-momentum $\mathbf{k}$, and $\hat{k}$ is the direction of $\mathbf{k}$.

APPENDIX B: THE TABLE OF MASS SPECTRUM OF SELECTED STATES IN THE PDG

The masses and widths of the meson states used in this work are listed in Table VI.

TABLE VI. The mass spectrum of quarkonium with those of candidates in the PDG [32]. The unit is MeV.

System	States	PDG states	PDG masses	PDG width	GI mass [31]
$u\bar{d}, \frac{1}{\sqrt{2}}(u\bar{u}-d\bar{d}), d\bar{u}$	1^1S_0	π	134.9/139.5	···	153
	1^3S_1	$\rho(770)$	775.26 ± 0.23	147.4 ± 0.8	771
	2^3S_1	$\rho(1450)$	1465 ± 25	400 ± 60	1456
	1^3D_1	$\rho(1700)$	1720 ± 20	250 ± 100	1664
	1^1P_1	$b_1(1235)$	1229.5 ± 3.2	142 ± 9	1219
	1^3P_1	$a_1(1260)$	1230 ± 40	380 ± 80	1238
	1^3P_2	$a_2(1320)$	1318.2 ± 0.6	107 ± 5	1307
	2^3P_2	$a_2(1700)$	1706 ± 14	380^{+60}_{-50}	1823
	1^1D_2	$\pi_2(1670)$	$1670.6^{+2.9}_{-1.2}$	258^{+8}_{-9}	1680
	1^3D_3	$\rho_3(1690)$	1688.8 ± 2.1	161 ± 10	1683
$u\bar{s}$, $d\bar{s}$, $s\bar{u}$, $s\bar{d}$	1^1S_0	K	497.6/493.7	···	463
	1^3S_1	$K^*(892)$	891.67 ± 0.26	51.4 ± 0.8	903
	1^3P_2	$K_2^*(1430)$	1427.3 ± 1.5	100.0 ± 2.2	1428
	1^3D_1	$K^*(1680)$	1718 ± 18	320 ± 110	1776
	1^3D_3	$K_3^*(1780)$	1779 ± 8	161 ± 17	1794
	1^3F_4	$K^*(2045)$	2048^{+8}_{-9}	199^{+27}_{-19}	2108
	1^3G_5	$K^*(2380)$	2382 ± 24	180 ± 50	2388
f'	1^1S_0	η	547.862 ± 0.017	1.31 ± 0.05	520
	1^3S_1	$\phi(1020)$	1019.460 ± 0.016	4.249 ± 0.013	1020
	1^3P_2	$f_2'(1525)$	1517.3 ± 2.4	72^{+7}_{-6}	1530
	1^3D_3	$\phi_3(1850)$	1854 ± 7	87^{+28}_{-23}	1900
f	1^1S_0	$\eta'(958)$	957.78 ± 0.06	0.188 ± 0.006	960
	1^3S_1	$\omega(782)$	782.66 ± 0.13	8.68 ± 0.13	780
	2^3S_1	$\omega(1420)$	1410 ± 60	290 ± 190	1460
	1^3P_2	$f_2(1270)$	1275.4 ± 0.8	$185.8^{+2.8}_{-2.1}$	1280
	1^3F_4	$f_4(2050)$	2018 ± 11	237 ± 18	2010

[1] L. Micu, Nucl. Phys. **B10**, 521 (1969).
[2] A. Le Yaouanc, L. Oliver, O. Pene, and J. C. Raynal, Phys. Rev. D **8**, 2223 (1973).
[3] A. Le Yaouanc, L. Oliver, O. Pene, and J. C. Raynal, Phys. Rev. D **9**, 1415 (1974).
[4] W. Roberts and B. Silvestre-Brac, Few Body Syst. **11**, 171 (1992).
[5] S. Capstick and W. Roberts, Phys. Rev. D **49**, 4570 (1994).
[6] S. Capstick and W. Roberts, Prog. Part. Nucl. Phys. **45**, S241 (2000).
[7] H. G. Blundell and S. Godfrey, Phys. Rev. D **53**, 3700 (1996).
[8] T. Barnes, F. E. Close, P. R. Page, and E. S. Swanson, Phys. Rev. D **55**, 4157 (1997).
[9] Q.-T. Song, D.-Y. Chen, X. Liu, and T. Matsuki, Phys. Rev. D **91**, 054031 (2015).
[10] J. Lu, X.-L. Chen, W.-Z. Deng, and S.-L. Zhu, Phys. Rev. D **73**, 054012 (2006).
[11] B. Zhang, X. Liu, W.-Z. Deng, and S.-L. Zhu, Eur. Phys. J. C **50**, 617 (2007).
[12] X.-C. Feng, Z.-Y. Li, D.-M. Li, Q.-T. Song, E. Wang, and W.-C. Yan, Phys. Rev. D **106**, 076012 (2022).
[13] T.-G. Li, Z. Gao, G.-Y. Wang, D.-M. Li, E. Wang, and J. Zhu, Phys. Rev. D **106**, 034012 (2022).
[14] Q.-T. Song, D.-Y. Chen, X. Liu, and T. Matsuki, Eur. Phys. J. C **75**, 30 (2015).
[15] D.-Y. Chen, Eur. Phys. J. C **76**, 671 (2016).
[16] Q. Li, L.-C. Gui, M.-S. Liu, Q.-F. Lü, and X.-H. Zhong, Chin. Phys. C **45**, 023116 (2021).
[17] C.-Q. Pang, Phys. Rev. D **99**, 074015 (2019).
[18] C.-Q. Pang, Y.-R. Wang, and C.-H. Wang, Phys. Rev. D **99**, 014022 (2019).
[19] L.-Y. Xiao, X.-Z. Weng, Q.-F. Lü, X.-H. Zhong, and S.-L. Zhu, Eur. Phys. J. C **78**, 605 (2018).
[20] J. Ferretti and E. Santopinto, Phys. Rev. D **97**, 114020 (2018).
[21] Z.-F. Sun and X. Liu, Phys. Rev. D **80**, 074037 (2009).
[22] H. Garcia-Tecocoatzi, A. Giachino, J. Li, A. Ramirez-Morales, and E. Santopinto, Phys. Rev. D **107**, 034031 (2023).

[23] E. S. Ackleh, T. Barnes, and E. S. Swanson, Phys. Rev. D **54**, 6811 (1996).
[24] R. Kokoski and N. Isgur, Phys. Rev. D **35**, 907 (1987).
[25] K. Heikkila, S. Ono, and N. A. Tornqvist, Phys. Rev. D **29**, 110 (1984); **29**, 2136(E) (1984).
[26] Y. S. Kalashnikova, Phys. Rev. D **72**, 034010 (2005).
[27] Z.-Y. Zhou and Z. Xiao, Phys. Rev. D **96**, 054031 (2017); **96**, 099905(E) (2017).
[28] M. G. Fuda, Phys. Rev. C **86**, 055205 (2012).
[29] Z.-Y. Zhou and Z. Xiao, Eur. Phys. J. C **80**, 1191 (2020).
[30] M. Jacob and G. C. Wick, Ann. Phys. (N.Y.) **7**, 404 (1959).
[31] S. Godfrey and N. Isgur, Phys. Rev. D **32**, 189 (1985).
[32] S. Navas *et al.* (Particle Data Group), Phys. Rev. D **110**, 030001 (2024).
[33] F. E. Close and N. A. Tornqvist, J. Phys. G **28**, R249 (2002).
[34] Y.-R. Wang, T.-Y. Li, Z.-Y. Fang, H. Chen, and C.-Q. Pang, Phys. Rev. D **106**, 114024 (2022).
[35] G.-Y. Wang, S.-C. Xue, G.-N. Li, E. Wang, and D.-M. Li, Phys. Rev. D **97**, 034030 (2018).
[36] P. Geiger and N. Isgur, Phys. Rev. D **55**, 299 (1997).
[37] A. D. Martin and T. D. Spearman, *Elementary Particle Theory* (North-Holland Publishing Co., Amsterdam, 1970).